Biosensors and Bioelectronics 39 (2013) 346–351

Contents lists available at SciVerse ScienceDirect

Biosensors and Bioelectronics

journal homepage: www.elsevier.com/locate/bios

Short communication

Real-time label-free immunoassay of interferon-gamma and prostate-specific antigen using a Fiber-Optic Localized Surface Plasmon Resonance sensor

Hyeon-Ho Jeong [a], Norov Erdene [b], Jae-Hyoung Park [c], Dae-Hong Jeong [b,d], Ho-Young Lee [a,e], Seung-Ki Lee [c,*]

[a] Department of Nuclear Medicine, SNU College of Medicine, Institute of Radiation Medicine, SNUMRC, 28 Yongon-Dong, Chongno-Gu, Seoul 110-799, Republic of Korea
[b] Nano Systems Institute-National Core Research Center (NSI-NCRC), Seoul National University, Seoul 151-742, Republic of Korea
[c] Department of Electronics and Electrical Engineering, Dankook University, Gyeonggi-do 448-701, Republic of Korea
[d] Department of Chemistry Education, Seoul National University, Seoul 151-742, Republic of Korea
[e] Department of Nuclear Medicine, Seoul National University Boramae Medical Center, 39 Boramae-Gil, Dongjak-Gu, Seoul 156-707, Republic of Korea

ARTICLE INFO

Article history:
Received 11 May 2012
Received in revised form
26 July 2012
Accepted 7 August 2012
Available online 16 August 2012

Keywords:
Fiber-Optic Localized Surface Plasmon Resonance (FO LSPR)
Interferon-gamma (IFN-γ)
Prostate-specific antigen (PSA)
Real-time detection
Label-free immunoassay
Fiber-optic sensor

ABSTRACT

A Fiber-Optic Localized Surface Plasmon Resonance (FO LSPR) sensor was fabricated using spherical gold nanoparticles (Au NPs) on a flattened end-face of the optical fiber. The Au NPs were easily synthesized by the Turkevich method and were immobilized on the end-face of the optical fiber by using a self-assembled monolayer (SAM). In order to examine the possibility of its application as a biosensor for label-free immunoassays, the fabricated FO LSPR sensor was used for the detection of the antibody–antigen reaction of interferon-gamma (IFN-γ) and the limit of detection (LOD) was approximately 2 pg/ml. Herein, The antibodies and bovine serum albumins (BSAs) were immobilized on the Au NPs by physisorption. Also, the FO LSPR sensor was used for the detection of a prostate-specific antigen (PSA) and the LOD was 1 pg/ml below. The fabricated FO LSPR sensor can be used for *real-time* label-free immunoassay having fast detection time, high resolution and sensitivity. In addition, the proposed sensor platform has the advantages of low cost, simple optical setup, remote sensing, simple fabrication, *real-time* detection, low sample volume, and potential application to in-vivo detection systems.

1. Introduction

Localized Surface Plasmon Resonance (LSPR) is a resonance phenomenon of free electron waves in metal nanoparticles (MNPs) and the nanometer-scale rough surface in the UV–vis range (Homola, 2003; Homola et al., 1999; Mulvaney, 1996; Underwood and Mulvaney, 1994). LSPR has the advantages of label-free detection, low sample volume, *real-time* detection, and simple optical setup (Jeong et al., 2011; Jeong and Lee, 2011; Lee et al., 2010a,2011). Fiber-Optic Localized Surface Plasmon Resonance (FO LSPR) is based on LSPR using MNPs on an optical fiber, which can deliver a lossless optical signal through total internal reflection (TIR) between the core and cladding parts (Jeong et al., 2011; Lee et al., 2010a). The most important step in the fabrication of an LSPR or FO LSPR sensor is the formation of the MNPs. The LSPR spectrum is changed by controlling the size (Bell and McCourt, 2009; Chen et al., 2008), density (Jeong et al., 2011), gap (Acimovic et al., 2009; Smythe et al., 2007), and shape (Chen et al., 2009; Haynes and Van Duyne, 2003; Huang et al., 2009; Smythe et al., 2007) of the MNPs, because the Localized Surface Plasmon (LSP) enhancement is altered by the distribution of the electric field on the MNPs. By designing the structure of the MNPs to maximize the enhancement of LSP, the sensitivity of the LSPR or FO LSPR sensor can be enhanced (Alleyne et al., 2007; Bell and McCourt, 2009). The Turkevich method for the synthesis of spherical Au NPs has been widely used, because it has the advantages of having a simple and fast fabrication process, while also having the ability to easily control the size of the gold nanoparticles (Au NPs) (Kimling et al., 2006; Lee et al., 2010a). Besides the synthesis of the spherical Au NPs, various shapes such as nanorods (Huang et al., 2009; Smythe et al., 2007; Ueno et al., 2006), nanocubes (Chen et al., 2009; Huang et al., 2006), bipyramids (Chen et al., 2008), etc., can be fabricated. In recent years, MNPs have been fabricated using Micro Electro Mechanical Systems (MEMS) technologies such as electron-beam lithography (EBL) (Acimovic et al., 2009; Barbillon et al., 2007; Smythe et al., 2007), nanoimprint lithography (NIL) (Jeong et al., 2010; Lee et al., 2011), nanosphere lithography (NSL) (Haes and Van Duyne, 2004;

* Corresponding author. Tel.: +82 31 8005 3607; fax: +82 31 8005 3622.
E-mail addresses: korea323@hotmail.com (H.-H. Jeong), erdene_ar@yahoo.com (N. Erdene), parkjae@dankook.ac.kr (J.-H. Park), jeongdh@snu.ac.kr (D.-H. Jeong), debobkr@gmail.com (H.-Y. Lee), skilee@dku.edu (S.-K. Lee).

0956-5663/$ - see front matter © 2012 Elsevier B.V. All rights reserved.
http://dx.doi.org/10.1016/j.bios.2012.08.013

Haynes and Van Duyne, 2003; Ormonde et al., 2004), and block copolymer lithography (BCPL) (Shin et al., 2010).

LSPR sensors have been used to detect the interactions of biomolecules such as antibody–antigen reactions (Jeong et al., 2011; Sai et al., 2009; Shao et al., 2010; Stybayeva et al., 2010; Tuleuova et al., 2010), DNA hybridization (Endo et al., 2005; Kim et al., 2007), etc. (Jeong and Lee, 2011; Mitsui et al., 2004). As an example, for the detection of the antibody–antigen reaction of a prostate-specific antigen (PSA) and an interferon-gamma (IFN-γ), antigen PSA and antigen IFN-γ were detected using various LSPR sensors (Besselink et al., 2004; Cao et al., 2006; Cao and Sim, 2009; Grubisha et al., 2003; Healy et al., 2007; Huang et al., 2005; Jang et al., 2009; Katsamba et al., 2006; Kim et al., 2005; Lee et al., 2011,2010b; Shin et al., 2010; Stybayeva et al., 2010; Tuleuova et al., 2010).

An FO LSPR sensor can be used as a portable sensor for chemical and biological detection, because it has the advantages of lossless signal delivery, remote sensing, low cost, and simple optical setup (Jeong et al., 2011; Lee et al., 2010a; Sharma et al., 2007). FO LSPR sensors have been fabricated with sensor surfaces having various shapes, such as a flattened tip (Jeong et al., 2011; Jeong and Lee, 2011; Mitsui et al., 2004; Smythe et al., 2007), sharp tip (Lee and Lee, 2008; Lee et al., 2008), and dumbbell shape (Lee et al., 2010a; Sai et al., 2009; Shao et al., 2010).

In this study, an FO LSPR sensor is fabricated using spherical Au NPs by the Turkevich method in order to reduce the cost, shorten the fabrication time, and facilitate the fabrication process with fiber-optics. The optical fiber is prepared with a flat structure, because of its simple fabrication, easy detection method, and the possibility for various applications, etc. The fabricated FO LSPR sensor is used to detect the antibody–antigen reaction of PSA and IFN-γ. The FO LSPR sensor for the detection of antigen PSA and antigen IFN-γ can be applied to in-vivo systems combined with an endoscope or laparoscope, because of its *real-time* label-free detection, miniaturized flatted tip, and fast sensitive detection.

2. Material and methods

2.1. Fabrication of FO LSPR sensor

In order to fabricate the FO LSPR sensor, Au NPs should be formed on the end-face of the optical fiber (Fig. 1A). A multimode optical fiber, for which the diameters of the core and cladding are 105 μm and 125 μm, respectively, was purchased from Thorlabs (AFS 105/125Y). The end-face of the optical fiber was designed to be perpendicular to the direction of the incident light using an optical fiber cleaver (FCP-22, Sumitomo Electric).

Au NPs were synthesized by reducing chloroauric acid ($HAuCl_4 \cdot 3H_2O$, 99%, Sigma Aldrich) (Jeong et al., 2011). In brief, 50 ml of a 0.01% (w/v) aqueous solution of $HAuCl_4$ was boiled on a hotplate at 100°C and 0.5 ml of 1% (w/v) sodium citrate (trisodium citrate tribasic dehydrate, 99%, Sigma Aldrich) was added in a boiling solution of 0.01% (w/v) $HAuCl_4$. After the solution was boiled with vigorous stirring for 20 min, the color of the solution changed from bright yellow to red (Fig. S1). In this method, the less sodium citrate added, the larger were the diameters of the Au NPs obtained. The average diameter of the synthesized spherical Au NPs was 35.1 ± 7.2 nm (Fig. 1A). We calculated the surface density ratio by analyzing the surface of the sensor using the FE-SEM image as shown in Fig. 1A. The surface density ratio was 31.3%. Herein, the surface density ratio is defined as the area of the Au NPs on the end-face of the FO LSPR sensor per area of the FE-SEM image.

The fabrication process of the FO LSPR sensor was divided into three steps (Fig. 1B). In the first step, the flattened optical fiber was immersed in a piranha solution, which is composed of sulfuric acid (H_2SO_4, 95%, Dae-jung Chemicals) and hydrogen peroxide (H_2O_2, 30%, Dae-jung Chemicals) at a volume ratio of 4:1, for 20 min in order to clean the end-face of the optical fiber and to form hydroxyl groups on it. In the second step, the cleaned end-face of the optical fiber was immersed in a 5% (v/v) 3-aminopropyldimetylethoxysilane (APMES, Sigma Aldrich) solution for 90 min to form a self-assembled

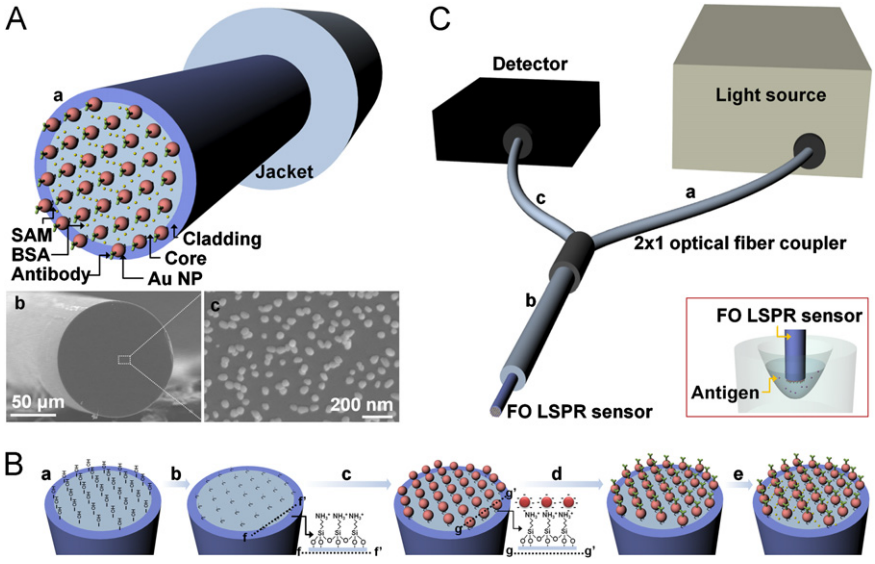

Fig. 1. (A) Illustration of the FO LSPR sensor (a), FE-SEM images of the end-face for the FO LSPR sensor (b) and the synthesized spherical Au NPs on the end-face of the fabricated FO LSPR sensor (c). The average diameter of the Au NPs was 35.1 ± 7.2 nm. The surface density ratio was 31.3%, which is defined as the ratio for the area of the Au NPs to the area of the SEM image in Fig. 1A. (B) Fabrication of the FO LSPR sensor and immobilization of the antibody and BSA on the end-face of the FO LSPR sensor: (a) hydroxyl functional groups were formed on the end-face of the optical fiber by dipping it in a piranha solution, (b) amino functional groups were formed on the hydroxyl functional groups by immersing the sensor in an APMES solution, (c) the Au NPs were immobilized on the SAM by immersing the sensor in a gold colloid solution, (d) the antibodies, antibody IFN-γ and antibody PSA, are adsorbed on the spherical Au NPs by physisorption, (e) the BSAs are adsorbed on the whole surface of the FO LSPR sensor in order to suppress the non-specific binding of the antigens with the surface of the sensor, except for the antibodies. (C) Schematic diagram of the optical measurement system with the FO LSPR sensor: a 2×1 optical fiber coupler was used, which has a Y connector on one side; one end of part (a) was connected with a light source for delivering the input signals, while the other end of part (b) was connected with a detector for receiving the reflected LSPR signals. At one end of the opposite side, part (c) was connected with the fabricated FO LSPR sensor.

monolayer (SAM) on it. Then, the end-face of the optical fiber was immersed in a gold colloid solution for 60 min to attach the Au NPs to it. In our previous study, we analyzed the sensitivities of the FO LSPR sensor for various diameters and densities of Au NPs on the end-face of the optical fiber and found the stable condition for its sensitivity and reproducibility (Jeong et al., 2011). In this study, the same condition was used for the diameter and density of the Au NPs.

2.2. Fabrication of the FO LSPR sensor for label-free immunoassay

The FO LSPR sensor used for the detection of the antibody–antigen reaction was fabricated using a two-step process (Fig. 1B). The first step is the immobilization of the antibody on the Au NPs immobilized on the surface of the fabricated FO LSPR sensor. The fabricated sensor was immersed in 100 μl of 20 μg/ml antibody, such as antibody IFN-γ (1.0 mg/ml purified Anti-Human IFN-γ, Becton Dickinson), capture antibody PSA (2.5 mg/ml, PSA 10), and tracer antibody PSA (2.4 mg/ml, PSA 66) mixed with a borate buffer (10 mmol, pH 8.5, GE Healthcare) for 15 min. The antibodies were mostly immobilized on the Au NPs of the end-face of the sensor, because the Au NPs have negative charges on their surface. On the other hand, the amino functional groups of the SAM, which are formed at the end-face of the sensor cause it to have positive charges on its surface (Zhou et al., 2009). Therefore, the binding force of the Au NPs with the antibody is stronger than that of the SAM on the surface of the sensor. In the second step, the surface of the sensor is treated with Bovine Serum Albumin (BSA, Sigma Aldrich) to suppress the nonspecific binding. The sensor was immersed in 100 μl of 1% BSA mixed with a 10 mmol borate buffer at pH 8.5 for 15 min. The BSA was adsorbed on the whole surface of the sensor except for the area covered by the antibody, and suppresses the binding of the antigen with the surface of the sensor except for the area covered by the antibody.

In order to confirm the immobilization process of the antibody and BSA, we measured the resonance signal during its overall process (Fig. S2). Each immobilization process of antibody IFN-γ, capture antibody PSA (PSA 10), and tracer antibody PSA (PSA 66) was proved by measuring the increase of the resonance signal step-by-step. Also, in order to verify the immobilization of antibody on the FO LSPR sensor, we used coomassie brilliant blue G 250 because of its high affinity with protein. The FO LSPR sensor was immersed in a staining solution, which contained coomassie brilliant blue dyes, for 1 h. After that, it was immersed in a destaining solution to remove the non-specific binding of coomassie brilliant blue dye with the surface of the FO LSPR sensor. Finally, it was washed by deionized water and its surface was observed through a microscope (Fig. S3).

2.3. Optical measurement system

The optical measurement system with the fabricated FO LSPR sensor is shown in Fig. 1C. In this optical system, a 2×1 optical fiber coupler was used, which has three light delivery paths. In Fig. 1C, part (a) and part (b) show the two ends on one side; one end was connected to the light source for delivering the input signals from the light source to the 2×1 optical fiber coupler, while the other end was connected to the detector for receiving the resonance signals reflected from the 2×1 optical fiber coupler to the detector. Part (c) shows one end on the opposite side, which was connected to the fabricated FO LSPR sensor using a fusion splicer (TYPE 35SE, Sumitomo Electric). In this study, two types of optical measurement systems were used, which use different light sources, viz. a white light source and a laser source. The first optical system uses a tungsten lamp as the white light source (AQ-4303B, ANDO) and a spectrometer (SM 200, Spectral products) as the detector to measure the resonance spectrum. The second optical system uses a 635 nm fiber coupled laser source (S1FC635, Thorlabs) and the detector is a photodetector (PDA36A, Thorlabs). The photodetector was used to measure the resonance intensity of the wavelength at 635 nm and the measured signal was transferred to a computer using a DAQ (USB 6008B, National Instruments).

3. Results and discussion

3.1. LSPR measurements

The measurement of the basic sensing characteristics for the fabricated FO LSPR sensor was conducted using deionized water, whose refractive index is 1.33, and five solutions with different refractive indices, viz. 1.34, 1.35, 1.36, 1.37, and 1.38 (Series AAA, Cargille Labs) as the sensing medium.

We measured the change of the resonance spectra for the various refractive indices using the white light, and plotted the resonance intensities at a wavelength of 635 nm for comparison with the results obtained using the 635 nm fiber coupled laser. Also, the resonance intensities of the FO LSPR sensor were measured using the laser and were plotted under the same conditions as those of the previous experiment. The results obtained from both the white light and laser experiments show a linear increase of the intensity when the refractive index is increased from 1.33 to 1.38 (Fig. 2A). The sensitivity of the fabricated FO LSPR sensor is defined as the change of the resonance intensity (ΔI) per unit change of the refractive index (Δn) and expressed as $S = \Delta I/\Delta n\ \mathrm{RIU}^{-1}$ as a function of the normalized resonance intensity. Herein, RIU means refractive index unit, and the normalized resonance intensity is the relative intensity for a refractive index of 1.33 as a reference (Jeong et al., 2011; Jeong and Lee, 2011). The sensitivity of the fabricated FO LSPR sensor is 27.5 RIU^{-1}.

3.2. Detection of antibody–antigen reaction of IFN-γ

We proved that the fabricated FO LSPR sensor can be used for *real-time* immunoassays by detecting the antibody–antigen reaction of IFN-γ. The FO LSPR sensor, which is bound with the antibody IFN-γ and BSA, was immersed in 100 μl of various concentrations of antigen IFN-γ (50 μg/100 μl Recombinant Human IFN-γ, Becton Dickinson) mixed with $1 \times$ PBS (addition of 1 mg/ml BSA) at pH 7.4 for 5 min. Fig. 2B shows the results of the resonance intensity at a wavelength of 635 nm for *real-time* detection using the 635 nm fiber coupled laser. It shows the sensorgram and the net change for various concentrations of antigen IFN-γ ranging from 0.1 pg/ml to 1 μg/ml. The range of concentrations of antigen IFN-γ was increased by ten times. In each case, the reaction time was 5 min and the resonance intensity was measured in $1 \times$ PBS at pH 7.4 for 5 min. Herein, the net change is defined as the difference between the normalized resonance intensities at various concentrations of antigen IFN-γ and the normalized resonance intensity at a concentration of antigen IFN-γ of 0 pg/ml. The result was fitted by Origin Pro 8 using the Dose Response Analysis method. The dynamic range of the fabricated FO LSPR sensor was measured to be from 2 pg/ml to around 500 pg/ml, which means that the limit of detection (LOD) is roughly 2 pg/ml and the maximum binding capacity is around 500 pg/ml. Previous results for the detection of antibody–antigen reaction of IFN-γ show the limit of detection of 100 pg/ml (SPR imaging system), 10 pg/ml (BIAcore-X SPR biosensor system), 0.54 nmol (~10 ng/ml) (LSPR sensor), 100 ng/ml (SPR instrument), and 10 pg/ml (FO LSPR sensor) (Jeong et al., 2011; Kim et al., 2005; Lee et al., 2010b; Stybayeva et al., 2010).

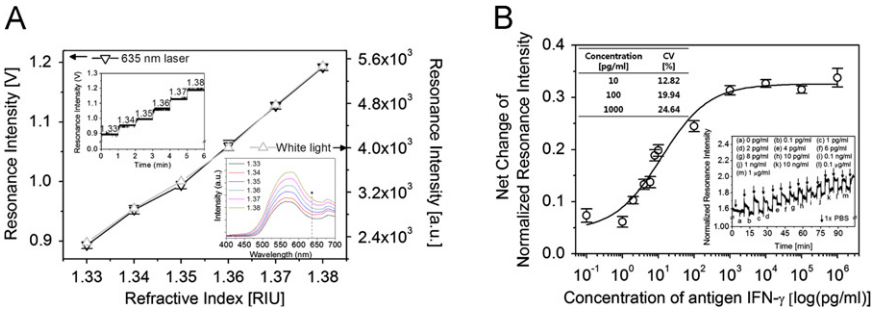

Fig. 2. (A) Resonance intensities for the various refractive indices at a wavelength of 635 nm: the refractive indices varied from 1.33 to 1.38 with 0.01 RIU intervals. The black triangles were measured by a 635 nm fiber coupled laser and each of the measured results was averaged using the measured resonance signals, as shown in the left inset. The resonance signals in the right inset were measured for various refractive indices using a white light source and the gray triangles mean the resonance intensities for various refractive indices at a wavelength of 635 nm. (B) The results of the antibody–antigen reaction of IFN-γ: Net change of the antibody–antigen reaction for the specific binding of antibody IFN-γ and antigen IFN-γ. Each of the data points means the normalized resonance intensity, which is the measured resonance signal at each concentration of antigen IFN-γ. The black line means the dose response curve fitted by Origin Pro 8 using the method of Dose Response Analysis. Inset: the bottom inset is the sensorgram for the antibody–antigen reaction of antigen IFN-γ with antibody IFN-γ to analyze the specific binding. The time allowed for the binding of antibody IFN-γ with various concentrations of antigen IFN-γ, viz. (a) 0 pg/ml, (b) 0.1 pg/ml, (c) 1 pg/ml, (d) 2 pg/ml, (e) 4 pg/ml, (f) 6 pg/ml, (g) 8 pg/ml, (h) 10 pg/ml, (i) 100 pg/ml, (j) 1 ng/ml, (k) 10 ng/ml, (l) 100 ng/ml and (m) 1 μg/ml, was approximately 5 min. Whenever the concentration of antigen IFN-γ was changed, the resonance signals were measured using 1 × PBS at pH 7.4 for 5 min to confirm the difference after the antibody–antigen reaction of IFN-γ. The upper inset is the table of the CVs for the net changes of the antibody–antigen reaction for IFN-γ, which were calculated by detecting the net changes for the concentrations of antigen IFN-γ for 10 pg/ml, 100 pg/ml, and 1 ng/ml twice. Each CV for the concentrations of antigen IFN-γ of 10 pg/ml, 100 pg/ml, and 1 ng/ml was 12.82%, 19.94%, and 24.64%, respectively.

The measured value of the LOD is lower than that of the reported biosensor for IFN-γ as shown in Table S1. The normalized resonance intensity means the relative intensity with the intensity of deionized water as the reference, which is therefore in dimensionless units (Jeong and Lee, 2011).

In order to investigate the reproducibility of the net changes for various concentrations of antigen IFN-γ, the resonance signals at the concentrations of IFN-γ of 10 pg/ml, 100 pg/ml, and 1 ng/ml were detected twice and each of its coefficient of variations (CVs) was 12.82%, 19.94%, and 24.64%, respectively (Fig. 2B upper inset).

Clinically, the normal level of IFN-γ is lower than 30 pg/mL and it could be elevated in some diseases by nearly 1 ng/mL (Caldas et al., 2005). From the detected results for the antibody–antigen reaction of IFN-γ using the fabricated FO LSPR sensor, the sensor is expected to be used to detect antigen IFN-γ on the clinical test.

3.3. Detection of antibody–antigen reaction of PSA

In order to detect the antibody–antigen reaction of PSA using the fabricated FO LSPR sensor, we used capture antibody PSA (PSA 10), tracer antibody PSA (PSA 66), and antigen PSA included in the commercialized ELISA kit. PSA 10 is used as the capture antibody, because it has good affinity with antigen PSA and PSA 66 is used as the tracer antibody, since it has good selectivity with antigen PSA. In this experiment, we detected the specific binding of antibody PSA with various concentrations of antigen PSA. Also, in order to confirm the result for the specific binding of antibody PSA with antigen PSA, we measured the non-specific binding of antibody PSA with various concentrations of antigen IFN-γ.

First, we measured the sensorgram for the specific binding of antibody PSA with antigen PSA (Fig. S4). The procedure of the antibody–antigen reaction of PSA was the same as that used for the detection of IFN-γ. Fig. S4A shows the sensorgram for various concentrations of antigen PSA with the capture antibody PSA. The FO LSPR sensor, which is bound with the capture antibody and BSA, was immersed in 100 μl of various concentrations regarding antigen PSA mixed with 1 × PBS (addition of 1 mg/ml BSA) at pH 7.4 for 5 min. The concentrations of antigen PSA were increased by ten times from 0.1 pg/ml to 10 ng/ml. In each case, the reaction time was 5 min and the resonance intensity was measured in 1 × PBS at pH 7.4 for 5 min. Fig. S4B shows the sensorgram for various concentrations of antigen PSA with tracer antibody PSA under the same conditions as those in Fig. S4A.

Fig. 3 A shows the net changes of the antibody–antigen reaction for the specific binding of antibody PSA and antigen PSA. The black line and triangles are the results for the specific binding of the capture antibody PSA with antigen PSA. Also, the gray line and triangles are the results for the specific binding of the tracer antibody PSA with antigen PSA. The lines were fitted by Origin Pro 8 using the method of Dose Response Analysis. Both results varied linearly from roughly 0.5 pg/ml to around 500 pg/ml, which means that the maximum binding capacity is around 500 pg/ml. The results obtained using capture antibody PSA were a little higher than those using tracer antibody PSA, because of its good affinity with antigen PSA. Previous results for the detection of antibody–antigen reaction regarding PSA show the limit of detection of 83 fmol (~3 pg/ml) (LSPR based on the Au nanodisks), 0.1 pg/ml (LSPR using dark-field spectroscopy), 0.1 μg/ml (Fiber-Optic Surface Plasmon Resonance: FO SPR), and ~100 pg/ml (LSPR based on the hemispherical MNPs) (Cao and Sim, 2009; Jang et al., 2009; Lee et al., 2011; Shin et al., 2010). The measured values of the LOD are lower than that of the reported biosensor for PSA as shown in Table S2. For the reproducibility of the net changes for various concentrations of antigen PSA, the resonance signals at the concentrations of IFN-γ of 10 pg/ml, 100 pg/ml, and 1 ng/ml were detected twice and each of its CVs was calculated (Fig. 3A inset).

In order to confirm the results for the specific binding of antibody PSA with antigen PSA, as shown in Figs. S4 and 3A, we measured the non-specific binding of antibody PSA with antigen IFN-γ. Fig. S5 shows the sensorgrams for the non-specific binding between antibody PSA and antigen IFN-γ. The procedure of the antibody–antigen reaction was the same as that in Fig. S4. The antigen was just changed from antigen PSA to antigen IFN-γ to examine the signal change for the non-specific binding. Fig. S5A shows the sensorgram for the various concentrations of antigen IFN-γ with capture antibody PSA and Fig. S5B shows the sensorgram for the various concentrations of antigen IFN-γ with tracer antibody PSA.

Fig. 3C shows the net changes of the antibody–antigen reaction for the non-specific binding of antibody PSA and antigen IFN-γ. The black triangles are the results for the non-specific binding of capture antibody PSA with antigen IFN-γ. Also, the gray triangles are the results for the non-specific binding of tracer antibody PSA with antigen IFN-γ. The results did not demonstrate any correlations with the changes for the various concentrations

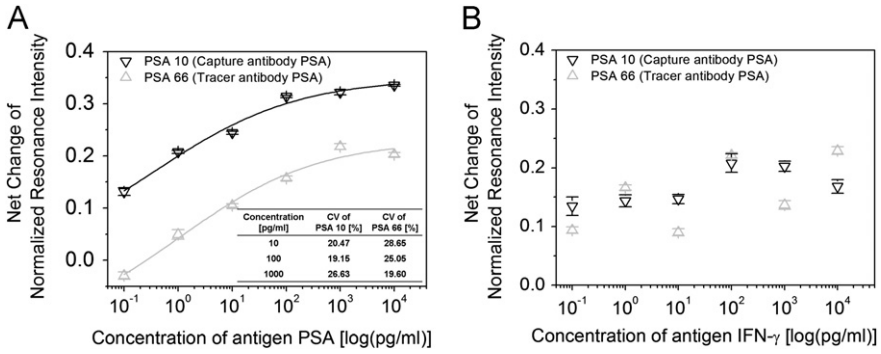

Fig. 3. (A) Net changes of the antibody–antigen reaction for the specific binding of antibody PSA and antigen PSA: The black line and triangles are the results for various concentrations of antigen PSA with capture antibody PSA (PSA 10). The gray line and triangles are the results for various concentrations of antigen PSA with tracer antibody PSA (PSA 66). Each of the triangles means the normalized resonance intensity, which is the measured resonance signal for each concentration of antigen PSA. The lines are the dose response curves, which were fitted by Origin Pro 8 using the method of Dose Response Analysis. Inset: the table of the CVs for the net changes for the antibody–antigen reaction of PSA, which were calculated by detecting the net changes for the concentrations of antigen PSA of 10 pg/ml, 100 pg/ml, and 1 ng/ml twice. In case of the capture antibody, each CV for the concentration of antigen PSA of 10 pg/ml, 100 pg/ml, and 1 ng/ml was 20.47%, 19.15%, and 26.63%, respectively. Also, in the case of the tracer antibody, each CV for the concentration of antigen PSA of 10 pg/ml, 100 pg/ml, and 1 ng/ml was 28.65%, 25.05%, and 19.60%, respectively. (B) Net changes of antibody–antigen reaction for the non-specific binding of antibody PSA with antigen IFN-γ: The black triangles are the results for various concentrations of antigen IFN-γ with capture antibody PSA (PSA 10). The gray triangles are the results for various concentrations of antigen IFN-γ with tracer antibody PSA (PSA 66). Each of the triangles signifies the normalized resonance intensity at each concentration of antigen IFN-γ.

of antigen IFN-γ, because of the non-specific binding of antibody PSA with antigen IFN-γ. These results mean that we detected the specific binding of antibody PSA with antigen PSA using the fabricated FO LSPR sensor and the specific binding of antibody PSA with antigen PSA was confirmed by measuring the non-specific binding of antibody PSA with antigen IFN-γ.

The reference range of the PSA level is lower than 4 ng/mL. However, the clinical significance of the PSA level is after prostatectomy. In this situation the change of a lower PSA level is important in order to detect early recurrence of prostate cancer (Taplin, 2003). For this reason, the fabricated FO LSPR sensor can be used to detect antigen PSA on the clinical test.

The maximum binding capacity of the fabricated FO LSPR sensor is dependent on the density of Au NPs on the end-face of the optical fiber. The density of the Au NPs on the end-face of the sensor is limited by the diameter of the core part in the optical fiber and it can be changed by varying the dipping time in the gold colloid solution. For this reason, the maximum binding capacity can be estimated by calculating the total number of Au NPs on the end-face of the FO LSPR sensor as it was around 300 pg/ml. The maximum binding capacity of the fabricated sensor can be enlarged by increasing the density of Au NPs or the diameter of the core part of the optical fiber, but the sensitivity of the sensor was decreased when the density of the Au NPs on the end-face of the optical fiber was increased in our previous research (Jeong et al., 2011). Therefore, the density of the Au NPs on the end-face of the optical fiber was fixed to maintain the optimized condition for the sensitivity of the FO LSPR sensor.

In order to improve the dynamic range and the reproducibility, the correlation between the dynamic range and the diameter of the core part in the optical fiber will be studied in the future. Also, the binding protocol for label-free immunoassay is being developed in order to enhance the stability and the reproducibility for the detected resonance signals using the fabricated FO LSPR sensor.

4. Conclusions

In this study, in order to investigate the possibility for *real-time* label-free immunoassays, an FO LSPR sensor was fabricated using spherical Au NPs and used to detect the antibody–antigen reaction of IFN-γ. Its dynamic range was about 2 pg/ml to approximately 500 pg/ml. The results for the antibody–antigen reaction of PSA as another application were also obtained for the specific binding of antibody PSA with various concentrations of antigen PSA. The measured results varied linearly around 0.5 pg/ml to around 500 pg/ml, which is the dynamic range of the fabricated FO LSPR sensor. Considering the clinical significance and situation, the fabricated FO LSPR sensor with the results for IFN-γ and PSA can be applied for clinical testing because it can rapidly detect the antibody–antigen reaction of PSA, as well as IFN-γ, with high resolution and sensitivity. In order to meet clinical validation, the binding protocol for label-free immunoassay is being developed to enhance the stability and the reproducibility for the net changes of the resonance signals. Also, the dynamic range of the FO LSPR sensor will be enlarged by increasing the diameter of the core part in an optical fiber and it will be used as a biosensor in order to detect IFN-γ and PSA in clinical samples.

Acknowledgment

This research was supported by the Pioneer Research Center Program through the National Research Foundation of Korea Funded by the Ministry of Education, Science and Technology (2012-0000448).

Appendix A. Supporting information

Supplementary data associated with this article can be found in the online version at http://dx.doi.org/10.1016/j.bios.2012.08.013.

References

Acimovic, S.S., Kreuzer, M.P., González, M.U., Quidant, R., 2009. ACS Nano 3 (5), 1231–1237.
Alleyne, C.J., Kirk, A.G., McPhedran, R.C., Nicorovici, N.-A.P., Maystre, D., 2007. Optics Express 15 (13), 8163–8169.
Barbillon, G., Bijeon, J.L., Plain, J., de la Chapelle, M.L., Adam, P.M., Royer, P., 2007. Surface Science 601 (21), 5057–5061.
Bell, S.E.J., McCourt, M.R., 2009. Physical Chemistry Chemical Physics 11 (34), 7455–7462.
Besselink, G.A.J., Kooyman, R.P.H., Os van, P.J.H.J., Engbers, G.H.M., Schasfoort, R.B.M., 2004. Analytical Biochemistry 333 (1), 165–173.
Caldas, A., Favali, C., Aquino, D., Vinhas, V., van Weyenbergh, J., Brodskyn, C., Costa, J., Barral-Netto, M., Barral, A., 2005. BMC Infectious Diseases 5 (1), 113.

Cao, C., Kim, J.P., Kim, B.W., Chae, H., Yoon, H.C., Yang, S.S., Sim, S.J., 2006. Biosensors and Bioelectronics 21 (11), 2106–2113.
Cao, C., Sim, S.J., 2009. Lab on a Chip 9 (13), 1836–1839.
Chen, H., Kou, X., Yang, Z., Ni, W., Wang, J., 2008. Langmuir 24 (10), 5233–5237.
Chen, H., Sun, Z., Ni, W., Woo, K.C., Lin, H.-Q., Sun, L., Yan, C., Wang, J., 2009. Small 5 (18), 2111–2119.
Endo, T., Kerman, K., Nagatani, N., Takamura, Y., Tamiya, E., 2005. Analytical Chemistry 77 (21), 6976–6984.
Grubisha, D.S., Lipert, R.J., Park, H.-Y., Driskell, J., Porter, M.D., 2003. Analytical Chemistry 75 (21), 5936–5943.
Haes, A.J., Van Duyne, R.P., 2004. Analytical and Bioanalytical Chemistry 379 (7), 920–930.
Haynes, C.L., Van Duyne, R.P., 2003. Nano Letters 3 (7), 939–943.
Healy, D.A., Hayes, C.J., Leonard, P., McKenna, L., O'Kennedy, R., 2007. Trends in Biotechnology 25 (3), 125–131.
Homola, J., 2003. Analytical and Bioanalytical Chemistry 377 (3), 528–539.
Homola, J., Yee, S.S., Gauglitz, G., 1999. Sensors and Actuators B: Chemical 54 (1–2), 3–15.
Huang, C.-J., Chiu, P.-H., Wang, Y.-H., Chen, W.R., Meen, T.H., 2006. Journal of the Electrochemical Society 153 (8), D129–D133.
Huang, L., Reekmans, G., Saerens, D., Friedt, J.-M., Frederix, F., Francis, L., Muylder-mans, S., Campitelli, A., Hoof, C.V., 2005. Biosensors and Bioelectronics 21 (3), 483–490.
Huang, X., Neretina, S., El-Sayed, M.A., 2009. Advanced Materials 21 (48), 4880–4910.
Jang, H.S., Park, K.N., Kang, C.D., Kim, J.P., Sim, S.J., Lee, K.S., 2009. Optics Communications 282 (14), 2827–2830.
Jeong, G.H., Park, J.K., Lee, K.K., Jang, J.H., Lee, C.H., Kang, H.B., Yang, C.W., Suh, S.J., 2010. Microelectronic Engineering 87 (1), 51–55.
Jeong, H.-H., Erdene, N., Lee, S.-K., Jeong, D.-H., Park, J.-H., 2011. Optical Engineering 50 (12), 124405–124408.
Jeong, H.-H., Lee, S.-K., 2011. Journal of Sensor Science and Technology 20 (2), 107–113.
Katsamba, P.S., Navratilova, I., Calderon-Cacia, M., Fan, L., Thornton, K., Zhu, M., Bos, T.V., Forte, C., Friend, D., Laird-Offringa, I., Tavares, G., Whatley, J., Shi, E., Widom, A., Lindquist, K.C., Klakamp, S., Drake, A., Bohmann, D., Roell, M., Rose, L., Dorocke, J., Roth, B., Luginbühl, B., Myszka, D.G., 2006. Analytical Biochemistry 352 (2), 208–221.
Kim, D.-K., Kerman, K., Saito, M., Sathuluri, R.R., Endo, T., Yamamura, S., Kwon, Y.-S., Tamiya, E., 2007. Analytical Chemistry 79 (5), 1855–1864.
Kim, M.-G., Shin, Y.-B., Jung, J.-M., Ro, H.-S., Chung, B.H., 2005. Journal of Immunological Methods 297 (1–2), 125–132.
Kimling, J., Maier, M., Okenve, B., Kotaidis, V., Ballot, H., Plech, A., 2006. The Journal of Physical Chemistry B 110 (32), 15700–15707.
Lee, H., Kim, H.J., Park, J.H., Jeong, D.H., Lee, S.K., 2010a. Measurement Science and Technology 21 (8), 085805.
Lee, H., Lee, S.-K., 2008. Journal of Korean Sensors Society 17 (2), 95–99.
Lee, J.-Y., Lee, C.-W., Lin, E.-H., Wei, P.-K., 2008. Applied Physics Letters 93 (17), 173110–173113.
Lee, S.-W., Lee, K.-S., Ahn, J., Lee, J.-J., Kim, M.-G., Shin, Y.-B., 2011. ACS Nano 5 (2), 897–904.
Lee, T.-H., Lee, S.-W., Jung, J.-A., Ahn, J., Kim, M.-G., Shin, Y.-B., 2010b. Sensors 10 (3), 2045–2053.
Mitsui, K., Handa, Y., Kajikawa, K., 2004. Applied Physics Letters 85 (18), 4231–4233.
Mulvaney, P., 1996. Langmuir 12 (3), 788–800.
Ormonde, A.D., Hicks, E.C.M., Castillo, J., Van Duyne, R.P., 2004. Langmuir 20 (16), 6927–6931.
Sai, V.V.R., Kundu, T., Mukherji, S., 2009. Biosensors and Bioelectronics 24 (9), 2804–2809.
Shao, Y., Xu, S., Zheng, X., Wang, Y., Xu, W., 2010. Sensors 10 (4), 3585–3596.
Sharma, A.K., Jha, R., Gupta, B.D., 2007. IEEE Sensors Journal 7 (8), 1118–1129.
Shin, D.O., Jeong, J.-R., Han, T.H., Koo, C.M., Park, H.-J., Lim, Y.T., Kim, S.O., 2010. Journal of Materials Chemistry 20 (34), 7241–7247.
Smythe, E.J., Cubukcu, E., Capasso, F., 2007. Optics Express 15 (12), 7439–7447.
Stybayeva, G., Kairova, M., Ramanculov, E., Simonian, A.L., Revzin, A., 2010. Colloids and Surfaces B: Biointerfaces 80 (2), 251–255.
Taplin, M.-E., 2003. Reviews in Urology 5 (2), S3–S13.
Tuleuova, N., Jones, C.N., Yan, J., Ramanculov, E., Yokobayashi, Y., Revzin, A., 2010. Analytical Chemistry 82 (5), 1851–1857.
Ueno, K., Juodkazis, S., Mizeikis, V., Sasaki, K., Misawa, H., 2006. Journal of the American Chemical Society 128 (44), 14226–14227.
Underwood, S., Mulvaney, P., 1994. Langmuir 10 (10), 3427–3430.
Zhou, J., Ralston, J., Sedev, R., Beattie, D.A., 2009. Journal of Colloid and Interface Science 331 (2), 251–262.